Environmental Science and Pollution Research (2023) 30:100095–100113
https://doi.org/10.1007/s11356-023-29377-w

RESEARCH ARTICLE

The efficient removal of ibuprofen, caffeine, and bisphenol A using engineered egusi seed shells biochar: adsorption kinetics, equilibrium, thermodynamics, and mechanism

René Blaise Ngouateu Lekene[1,2] · Tobie Matemb Ma Ntep[2] · Marcus N. A. Fetzer[2] · Till Strothmann[2] · Julius Ndi Nsami[1] · Christoph Janiak[2]

Received: 24 May 2023 / Accepted: 13 August 2023 / Published online: 25 August 2023

Abstract

Contaminants of emerging concern (CECs), also known as micropollutants, have been recognized in recent years as substantial water pollutants because of the potential threats they pose to the environment and human health. This study was aimed at preparing biochar (BC) based on egusi seed shells (ESS) with well-developed porosity and excellent adsorption capacity towards CECs including ibuprofen (IBP), caffeine (CAF), and bisphenol A (BPA). BC samples were prepared by pyrolysis at different temperatures (400 to 800 °C) and were characterized using nitrogen sorption, FTIR, powder X-ray diffraction (PXRD), SEM/EDS, elemental analysis, and thermal analysis. The nitrogen sorption and SEM results showed that the textural properties were more prominent as the pyrolysis temperature increased. The BC sample obtained at 800 °C which exhibited the largest specific surface area (688 m^2/g) and the highest pore volume (0.320 cm^3/g) was selected for the adsorption study of CECs. The kinetic study shows that the adsorption equilibrium of CAF and BPA was faster than that of IBP. The pseudo-first- and pseudo-second-order kinetic models best fitted the adsorption data. The Langmuir maximum monolayer adsorption capacities of biochar were found to be ~ 180, 121, and 73 mg/g respectively for IBP, CAF, and BPA. The thermodynamic study shows that the adsorption process was spontaneous and endothermic for the three CECs. The results of the adsorption and the analysis of BC after adsorption showed that hydrogen bonding, van der Waals, π-π, n-π interactions, and pore filling were involved in the adsorption mechanism. The prepared biochar BC from ESS displayed a large surface area and good morphology and significantly promotes adsorption of CECs and good efficiency on synthetic effluent. Finally, it offers a low-cost and cleaner production method.

Keywords Egusi seed shells · Biochar · Specific surface area · Contaminants of emerging concern · Wastewater treatment · Adsorption mechanism

Introduction

In recent decades, the rapid world population growth and industrial demand have led to increased consumption and contamination of natural waters by thousands of chemical compounds, including organic compounds such as antibiotics, persistent organic pollutants, pharmaceuticals, personal care products, and endocrine-disrupting chemicals (Gogoi et al. 2018). These compounds have been classified as micropollutants, contaminants of emerging concern (CECs), emerging pollutants (EPs), or emerging contaminants (ECs) depending on the authors due to their potential inherent capacity to produce harmful effects both on natural environments and living organisms including human health (Galindo-Miranda et al. 2019; Arman et al. 2021; Cheng et al. 2021; Kozyatnyk et al. 2021). CECs found in groundwater, surface water, marine ecosystems, landfill leachates, food sources, and natural water mainly come from anthropogenic activities. Their extensive occurrence, persistence, bioaccumulation, constant circulation, migration,

Responsible Editor: Tito Roberto Cadaval Jr

✉ René Blaise Ngouateu Lekene
lekeneblaise@yahoo.fr

[1] Applied Physical and Analytical Chemistry Laboratory, Department of Inorganic Chemistry, Faculty of Science, University of Yaoundé I, P.O. Box 812, Yaoundé, Cameroon

[2] Institut für Anorganische Chemie und Strukturchemie, Heinrich-Heine-Universität, Düsseldorf 40204, Germany

and transformation in environmental media have generated a huge global concern (Werkneh et al. 2022). Caffeine (CAF) is a psychotropic substance employed as an adjuvant analgesic and appetite suppressant as well as breathing stimulant (Correa-Navarro et al. 2022) and is found in medicines, drinks (soft drinks, coffee, and tea) and foods (dairy desserts, sweetmeats, and chocolates) (Zanella et al. 2021). Bisphenol A (BPA), considered one of the most produced industrial chemical compounds in the world, is an important starting material used for the production of plastic bags and could be transferred to packed food in case of incomplete polymerization (Antero et al. 2019; Tang et al. 2022), whereas ibuprofen is one of the world's most used medicine to treat rheumatic diseases, migraines, fever, muscles, and toothaches (Naima et al. 2022). All these three chemicals are frequently found in water bodies and are considered CECs without any real established standard. Nevertheless, the legislation is diverse depending on the country (Souza et al. 2021).

Recent scientific research focuses on advanced methods for the removal of CECs in water including electrochemical methods (Barrios et al. 2016), membrane processes (Acero et al. 2015), microbial methods (Ferreira et al. 2016), and advanced oxidation processes (Siara et al. 2022). However, these treatment methods show many drawbacks such as the generation of lethal by-products and high implementation cost. Several positive and promising results from published works report that the adsorption-based method was found to be affordable, suitable, and efficient in a wide range of CEC removal. Moreover, this technic offers the possibility to regenerate the adsorbent, minimizing lethal by-products to a great extent (Cheng et al. 2021; Naima et al. 2022; González-Hourcade et al. 2022). For the removal of organic and inorganic pollutants from aqueous media, the most studied adsorbent material is activated carbon. Despite its good adsorption performances, its utilization at large scale is still restricted for wastewater treatment due to its higher production cost (800 to 5000 USD/ton) from nonrenewable feedstock such as fossil coal, the use of harmful chemicals such as phosphoric acid or potassium hydroxide which may have a negative fingerprint on the environment, and high energy demand for the activation process (Kozyatnyk et al. 2021; Gurav et al. 2022). Therefore, the development of low-cost and environmentally friendly carbonaceous adsorbent material using renewable organic resource feedstock such as agricultural by-products is necessary for suitable and sustainable wastewater treatment systems.

Biochar (BC), a low-cost alternative for the replacement of fossil-based activated carbon for wastewater treatment, is a carbonaceous material obtained from the thermochemical conversion of biomass such as sewage sludge, animal manure, agricultural by-products, algae, and some few wood species in an oxygen-free atmosphere (Liao et al. 2022; Correa-Navarro et al. 2022). In order to tailor the physicochemical properties and the yield of BC, the pyrolysis procedure of feedstock can be either fast, intermediate, or slow depending on the heating rates and residential time (Hung et al. 2017). Initially, BC was prepared by pre-Columbian Amazonians for soil amendment and remediation to increase its fertility. Later on, due to its attractive properties such as abundant surface functional groups, large specific surface area, good porosity, low thermal conductivity, high chemical stability (to acidic and basic conditions), and low flammability, the use of BC was extended to other applications including wastewater treatment, energy storage, animal farming, carbon sequestration, anaerobic digestion, composting, construction, flue gas treatment, and climate change mitigation (Wang et al. 2020; Osman et al. 2022). In the particular case of water and wastewater treatment, it has been reported that biochar presents good efficiency towards removal of heavy metals (Ji et al. 2022), pesticides, dyes (Tran et al. 2017a; Hadj-Otmane et al. 2022), microplastics (Abuwatfa et al. 2021), and CECs including naproxen, diclofenac, and ibuprofen (Li et al. 2019; Cheng et al. 2021; Czech et al. 2021; Jha et al. 2023).

Cucumeropsis mannii N., commonly known as egusi, is an annual crop that belongs to the large family of Cucurbitaceae and which is cultivated for its seed in many Sub-Saharan African countries and mainly in Cameroon and Nigeria (Lékéné et al. 2018). The processing of egusi to obtain seeds leads to the generation of huge amounts of egusi seed shells (ESS) which are usually discarded as waste. Very few reported works mention the valorization of ESS. It has been used in our previous works as starting material for the preparation of activated carbon and its surface modification for nitrate ion removal (Lékéné et al. 2018; Lekene et al. 2021). Very recently, Popoola et al. studied the corrosion inhibition efficiency of its extract on carbon steel (Popoola et al. 2022). To the best of our knowledge, we herein present the first biochar obtained from egusi seed shells as raw material and for the removal of CECs from an aqueous solution. The ESS used to be burned in the open air leading to the production of nonneglectable amounts of carbon dioxide, the main component of greenhouse gas which is an environmental threat. The conversion of ESS to BC will address solid disposal issues, enhance its economic value, and also reduce the environmental fingerprint.

This study is aimed at highlighting the preparation of biochar based on egusi seed shells as starting raw material and at evaluating its affinity towards three selected CECs (ibuprofen, caffeine, and bisphenol A) in water. Various techniques were used to characterize the prepared biochars, namely, nitrogen sorption, Fourier-transform infrared spectroscopy (FTIR), powder X-ray diffraction (PXRD), scanning electron microscopy coupled with energy-dispersive X-ray spectroscopy (SEM/EDS),

elemental analysis (CHNS), thermogravimetric analysis (TGA), and pH of point of zero charges (pH_{PZC}). Batch experiments were used to evaluate the adsorption capacities, isotherm, and kinetics of the prepared biochar with varying operational conditions such as initial pH, contact time, initial CECs concentration, adsorbent dose, temperature, and desorbing agent. An adsorption mechanism has been suggested based on the properties of the biochar before and after the adsorption of CECs.

Materials and methods

Chemicals and reagents

All chemicals were used as received without further purification. Caffeine ($C_8H_{10}N_4O_2$, 99%) and bisphenol A ($C_{15}H_{16}O_2$, > 97%) were obtained from Alfa Aesar; ibuprofen ($C_{13}H_{18}O_2$, > 98%) was received from Tokyo Chemical Industry. Absolute ethanol (C_2H_6O), methanol (CH_4O, 99.8%), sodium chloride (NaCl, > 99%) hydrochloric acid (HCl, 37%), and sodium hydroxide (NaOH, > 98%) were purchased from Sigma-Aldrich. The physicochemical properties and chemical structure of CECs are given in the supplementary information (Table S1). Deionized water was used to prepare all aqueous solutions.

Biochar preparation

Egusi seed shells collected from the local market in the central region of Cameroon were used as precursors for preparation of BC. The raw material was washed several times with tap water to remove all dust and other impurities present at the surface, then rinsed with deionized water, and oven-dried at 105 °C. The dried ESS were crushed and screened with a 210-µm-diameter sieve before pyrolysis. Twenty grams of biomass was placed in a ceramic crucible with a lid and pyrolyzed in a muffle furnace (Carbolite Chamber Furnace, Germany), without using nitrogen or any inert gas for 1 h at different selected temperatures (400, 500, 600, 700, and 800 °C) at a heating rate of 10 °C/min (Fig. S1). The obtained biochars were washed several times with hot deionized water and oven-dried at 105 °C for 24 h. The biochars were then ground using an agate mortar and pestle followed by sieving to obtain particle sizes of less than 100 µm. Afterward, the products were sealed in a plastic container and stored in a desiccator for further use. Based on the pyrolysis temperature, the samples were named BC-400, BC-500, BC-600, BC-700, and BC-800. Each sample of biochar was produced in duplicate, and the mass yield was calculated using Eq. (1).

$$\text{Mass yield}(\%) = \frac{\text{Mass of obtained biochar (g)}}{\text{Mass of raw material (g)}} \times 100\% \quad (1)$$

Characterization methods

The prepared biochars were characterized before and after the adsorption of CECs using different techniques. After 16 h of outgassing under high vacuum at 120 °C, the specific surface area and pore size of the samples were determined by N_2 adsorption–desorption isotherm at 77 K using a Quantachrome Autosorb-6 instrument and calculated by BET and DFT methods, respectively. The PXRD patterns of the samples were obtained using a Rigaku MiniFlex X-ray diffractometer with Cu-Kα radiation (1.54182 Å) in the 2θ range of 2–100°. Fourier transform infrared (FTIR) spectroscopy (FT-IR Bruker Tensor 37) with KBr pellets was used to determine the surface functional groups of the BCs. FTIR spectra were recorded in transmittance mode in the range of 4000 cm^{-1} and 400 cm^{-1} with a resolution of 2 cm^{-1}. The surface morphology was assessed using a JEOL JSM-6510 scanning electron microscope with a LaB6 cathode at 20 kV equipped with a Bruker XFlash 410 silicon drift detector for energy-dispersive X-ray spectrometric (EDX) elemental composition analysis. Before image acquisition, the samples were coated with gold using a JEOL JFC-1200 Fine Coater. For SEM–EDX, the samples were glued on a carbon tape on top of a brass sample holder. Thus, the signals of C, Cu, Zn, and Au found in the EDX spectra are due to the carbon tape, the brass sample holder, and the sputtering of the sample with gold prior to the investigation. Thermogravimetric analysis (TGA) data were acquired with a NETZSCH TG 209 F3 Tarsus device by heating the samples from 30 to 1000 °C in the aluminum oxide crucible at a rate of 10 °C/min under a nitrogen flow of 20 mL/min. The carbon, hydrogen, nitrogen, and sulfur analyses were obtained using an Elementar Analysensysteme vario MICRO cube equipment. All samples were oven dried at 105 °C for 12 h. The drift method was used to assess the pH of the point of zero charge (pHpzc) as described by Correa-Navarro et al. (Correa-Navarro et al. 2022) (Supplementary information Section 1). The concentration of IBP, BPA, and CAF was determined using a double beam UV–vis spectrophotometer (VWA, P9) at maximum absorption wavelengths of 223.0, 276.6, and 272.0 nm respectively based on the absorption spectrum which was established beforehand.

Adsorption studies of CECs

IBP, BPA, and CAF removal studies were conducted in batch mode at ambient temperature (22 ± 2 °C). Closed vials containing a given amount of biochar and 10 mL of the CEC solution were shaken on the multipoint magnetic stirrer (Variomag, model HP 15) at 200 rpm for 4 h to investigate the effect of parameters such as pH (3–11), adsorbent dose (5–50 mg), and initial concentration (30–330 mg/L). The pH of the CEC solutions was adjusted using 0.1 mol/L of either sodium hydroxide or hydrochloric acid. The kinetics of the CEC adsorption was carried out using 100 mL of a solution containing 30 mg/L of contaminants and 100 mg of BC. The glass containers were shaken at 200 rpm for 7 h, and sampling was done at regular time intervals. The effect of temperature (30–50 °C) was also investigated in this study. After adsorption, the BC was separated from the dispersions by filtration using a 0.22-µm membrane syringe filter. The quantity adsorbed at equilibrium (q_e, mg/g) and at a given time (q_t, mg/g) along with the removal percentage (%R) was obtained using the following Eqs. (2)–(4), respectively:

$$q_e = \frac{(c_0 - c_e)}{m} \times V \tag{2}$$

$$q_t = \frac{(c_0 - c_t)}{m} \times V \tag{3}$$

$$\%R = \frac{(c_0 - c_e)}{C_0} \tag{4}$$

where c_0, c_t, and c_e are the CEC concentration (mg/L), at the beginning, any time t, and equilibrium respectively; V is the volume (L) of a solution; and m (g) the mass of the biochar.

The three CEC adsorption experiments were carried out in triplicate and the results are presented as the average of triplicate ± standard deviation (error bars). The parameters of the adsorption kinetics and adsorption isotherm were calculated by applying the trial-and-error nonlinear methods using the Solver add-in of the Microsoft Excel software. The best-fit models were identified by the calculations of the correlation coefficient (R^2), root-mean-square error (RMSE), and chi-square (χ^2) given by Eqs. (5)–(7) (Lekene et al. 2023).

$$R^2 = 1 - \frac{\sum_{i=1}^{n}\left(q_{e.\exp} - q_{e.\mathrm{pre}}\right)^2}{\sum_{i=1}^{n}\left(q_{e.\exp} - \overline{q_{e.\exp}}\right)^2} \tag{5}$$

$$\mathrm{RMSE} = \sqrt{\frac{\sum_{i=1}^{n}\left(q_{e.\exp} - q_{e.\mathrm{pre}}\right)^2}{n-1}} \tag{6}$$

$$\chi^2 = \sum_{i=1}^{n}\frac{\left(q_{e.\exp} - q_{e.\mathrm{pre}}\right)^2}{q_{e.\exp}} \tag{7}$$

where $q_{e.\mathrm{pre}}$, $q_{e.\exp}$ are the q_e values of the predicted and experimental values, respectively; n is the number of experimental runs.

Regeneration studies

For desorption efficiency investigation, adsorption was conducted using 250 mg of biochar and 100 mL of CEC with a concentration of 100 mg/L at the natural pH of each solution for 2 h. The CEC-loaded biochars were gently rinsed with deionized water to remove the unadsorbed CEC molecules and dried at 80 °C for 12 h. For desorption the study, 10 mg of the loaded biochar was stirred with 4 mL of desorbing agent including deionized water, ethanol, NaCl (0.1 mol/L), methanol, HCl (0.1 mol/L), and NaOH (0.1 mol/L) separately for 1 h.

Treatment of synthetic effluent

Generally, real effluents (hospitals) contain several inorganic and organic species that may affect the removal of the

Table 1 Chemical content and concentration of species in synthetic effluents

Effluent content species	Concentration (mg/L)	
	Effluent A	Effluent B
Pharmaceutical		
Caffeine	15	30
Ibuprofen	15	30
Paracetamol	10	20
Ciprofloxacin	10	20
Acetylsalicylic acid	10	20
Diclofenac	10	20
Sugar		
Saccharose	30	50
Other organic species		
Bisphenol A	15	30
Ammonium acetate	10	20
Urea	10	20
Inorganic species		
Ammonium sulfate iron	10	20
Ammonium phosphate	20	30
Calcium carbonate	10	30
Sodium chloride	50	70
Sodium hydrogencarbonate	10	20
pH*	6.94	7.11

*Without adjustment

targeted pollutant. Two solutions with different compositions (Table 1) were prepared by spiking deionized water with several chemicals in other to mimic real effluents and verify the efficiency of the prepared BC in real conditions (Lima et al. 2019; González-Hourcade et al. 2022). Twenty milliliters of synthetic effluents was added to a closed vial containing 40 mg of biochar displaying the best adsorption performance towards the targeted pollutants and stirred for 2 h. The UV–visible spectra of synthetic effluents before and after adsorption were recorded in the range of 190 to 400 nm and used to estimate the removal percentage of all the chemical species (Lima et al. 2019; González-Hourcade et al. 2022).

Results and discussion

Biochar physicochemical properties

The preparation of BC by pyrolysis at different temperatures of ESS yielded materials with different physical and chemical characteristics. As the pyrolysis temperature increased from 400 to 800 °C, the yield declined progressively from 42 to 26% (Table 2) as a result of the liberation of water and volatile matter coming from the decomposition of the biomass constituents (cellulose, hemicellulose, and lignin) under formation of CH_4, CO, H_2, and CO_2 at higher temperature (Chaves Fernandes et al. 2020; Veiga et al. 2020). The increase of the ash content from 10 to 18% as the temperature increases is due to the accumulation of minerals containing such as Cl, Ca, K, and Mg as seen on the EDX results (Fig. S2).

Figure 1a and b show the thermogravimetric (TGA) and derivative thermogravimetric (DTG) curves of the egusi seed raw material and of the derived biochars in the temperature range of 30 to 1000 °C under an inert atmosphere and heating rate of 10 °C/min. The first mass loss which occurs between 30 and 200 ℃ and does not exceed 8 wt% for all the samples was assigned to the vaporization of the moisture and the onset of the decomposition of biomass. In the case of the raw biomass material (ESS), the main mass loss of about 58 wt% observed between 200 and 400 °C can be attributed to the decomposition of cellulose, the main constituent of ESS with a peak temperature of 330 °C as shown by DTG (Veiga et al. 2020; Oginni and Singh 2021). For the prepared biochar materials, the important mass loss took place in the temperature range of 400 to 1000 °C, and, expectedly, the percentage of mass loss decreased as the pyrolysis temperature increased. For the BC-800 sample, the TGA curve gives a mass loss of only 31 wt% up to 1000 °C. The mass loss above 400 °C is associated with the degradation and decomposition of lignin and some inorganic species such as $CaCO_3$, K, and Mg (Veiga et al. 2020). The residual mass of the biochar at 1000 °C was approximately 11, 34, 40, 51, and 69% for BC-400, BC-500, BC-600, BC-700, and BC-800 respectively, along with the already higher degree of carbonization of the biochar.

The elemental composition of biochars given by CHNS analysis (Table 2) obviously depends on the pyrolysis temperature. As the temperature increases from 400 to 800 °C, the carbon content also increases from about 67 to 78% respectively while the opposite trend is observed for both hydrogen and oxygen contents. The increase in mass fraction of carbon along with the increase in temperature

Table 2 Physicochemical properties of prepared biochar at different temperatures

Parameters	Samples					
	ESS	BC-400	BC-500	BC-600	BC-700	BC-800
Yield (%)	/	42.48	34.40	31.55	29.36	26.25
Ash (%)	4.13	10.27	11.86	12.01	14.03	17.63
C	47.02	67.48	73.04	77.52	79.94	77.73
H	5.46	3.46	3.04	2.66	2.17	1.97
N	3.16	0.41	0.46	0.45	0.44	0.47
O[a]	40.23	18.38	11.60	7.36	3.42	2.20
Atomic ratio H/C	0.12	0.05	0.04	0.03	0.03	0.03
Atomic ratio O/C	0.86	0.27	0.16	0.09	0.04	0.03
pH_{pzc}	/	5.3	6.4	7.2	7.3	7.4
Surface area (m^2/g)[b]	5	11	90	476	558	688
Total pore volume (cm^3/g)[c]	0.00	0.02	0.06	0.22	0.29	0.35
Micropore volume (cm^3/g)[d]	0.00	0.00	0.03	0.18	0.22	0.27

[a]%O = 100 − (%C + %H + %N + %ash)

[b]Calculated BET surface area over the pressure range 0.02–0.06 P/P_0

[c]Total pore volume at $P/P_0 = 0.98$ for pores ≤ 20 nm

[d]Micropore volume calculated from N_2 adsorption isotherm at $P/P_0 = 0.1$ for pores with $d \leq 2$ nm (20 Å)

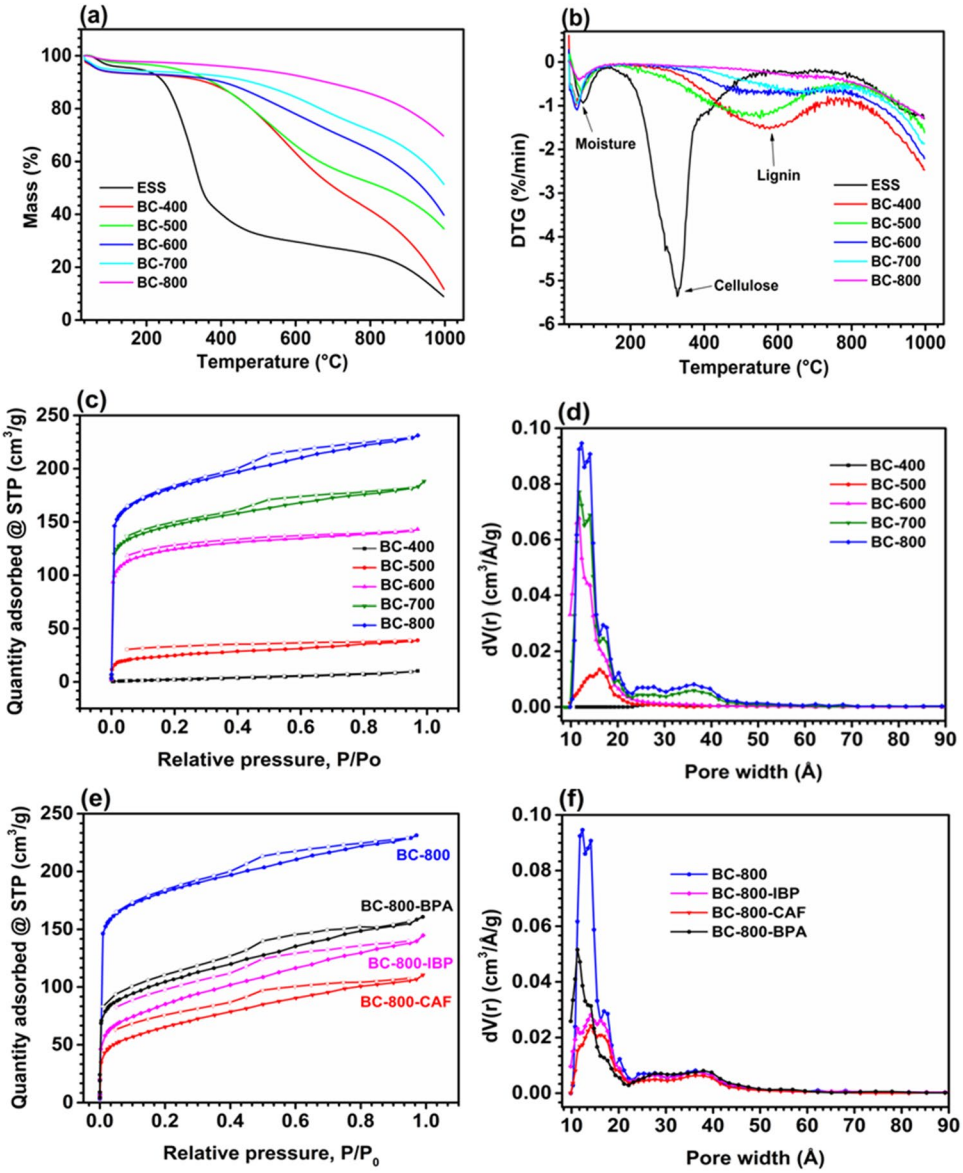

Fig. 1 **a** TGA and **b** DTG of raw material (ESS) and the derived biochars at different temperatures; nitrogen adsorption/desorption isotherm at 77 K of **c** BCs and **e** BC-800 after adsorption of CECs; pore size distribution of **d** BCs and **f** BC-800 after adsorption of CECs

can be attributed to the formation of graphitized carbon structure through polymerization and aromatization (Sahoo et al. 2021) while the decrease of hydrogen from ~ 4 to ~ 2% is due to increasing dehydration, cleavage, and cracking of C-H and O–H bonds, leading to the higher formation of aromatic structures (Oginni and Singh 2021). The release of oxygen and hydrogen as water vapor, CH_4, CO_2, and CO increases of the percentage of residual carbon. The nitrogen content of biochars is significantly affected by the pyrolysis temperature (from 3% in starting material to less than 0.5 % in BCs), while the sulfur was below the detection limit. The lower H/C and O/C molar ratio indicates the higher degree of aromaticity and carbonization of the carbonaceous material such that the aromaticity increases with the temperature (Ji et al. 2022). The decrease in the O/C ratio suggests that, as the pyrolysis increases, the surfaces of prepared biochar become more hydrophobic (Elnour et al. 2019).

Nitrogen adsorption/desorption measurements at 77 K of the biochars and the raw materials are given in Fig. 1 c and d and Fig. S3 respectively. BC-400 presents a type III isotherm with H3 hysteresis indicating that the sample is mainly macroporous. On the other hand, BC-500 to 800 materials all show type I(b) isotherms. Type I(b) isotherms are given by materials with pore size distributions over a broader range including wider micropores and narrow mesopores. BC-700 and BC-800 exhibit an H4 hysteresis characteristic of micro- to mesopores where the step-down of the desorption branch is located at P/P_0 ~ 0.4–0.5 (Thommes et al. 2015). For BC-500 and BC-600, the hysteresis loop closes only at a low relative pressure and may be associated with the change in volume of nitrogen due to the pore-blocking

effect (Maziarka et al. 2021). The specific BET surface area (11–688 m^2/g) and the pore volume (0.02–0.35 cm^3/g) increased with the pyrolysis temperature (Table 2). The low specific surface area of 11 m^2/g for BC-400 which is essentially the outer surface of a fine powder reflects the still largely preserved nonporous structure of the egusi seed shells (Sun et al. 2021; Ji et al. 2022); this observation was consistent with SEM analysis (Fig. 2). The main pore widths (diameters) of the biochar samples lie in the micropore (< 2 nm) region between 10 and 20 Å (Fig. 1d). Thereby, it should be noted that small micropores below 10 Å are difficult to probe with nitrogen at the cryogenic temperature of 77 K as diffusion of N_2 molecules into small micropores is very slow. The samples BC-700 and -800 also feature an increasing fraction of mesopores up to 45 Å, with the main porosity contribution still coming from the micropores (Fig. 1d). The biochars prepared from egusi seed shells in the present work show higher specific surface areas and pore volumes than that most of the biochar from other source reported in the literature (Table S2).

The SEM images of the raw biomass and biochar prepared at different temperatures are shown in Fig. 2. The raw biomass sample of ESS was observed to have a gentle surface with no pores as shown in Fig. 2a. All the biochar samples have random and irregular-shaped structures with sharp-edged particles possessing various sizes and with a rough surface. The sample obtained at the lowest temperature, BC-400 (Fig. 2b), shows almost no pores confirming or justifying its lowest specific surface area. As the temperature increases from 500 to 800 °C (Fig. 2c–f), highly macroporous honeycomb-like structures are created. These observations are in line with an increasing porosity given by the BET surface area and total pore volume. The macropore volume seen in the SEM images cannot be probed by N_2 sorption. However, as the pyrolysis temperature increases, the appearance of pores and channels became more prominent due to the release of more volatile matter which leads to the formation of pores of all sizes.

The FTIR spectra depicted in Fig. 3a show the general decrease in surface functional groups of ESS and biochars as the pyrolysis temperature increases. This can be attributed to the breakdown of various functional groups due to the removal of volatile matter and the concomitant degree of carbonization at higher pyrolysis temperatures (Elnour et al. 2019; Hadj-Otmane et al. 2022). Surface functional groups specific to an organic material have been identified. The broad peak at 3422 cm^{-1} corresponds to –OH stretching vibrations in phenols, alcohols, carboxylic, or absorbed water. The weak peaks at 2921 and 2860 cm^{-1} indicate the symmetric and asymmetric stretching vibration of C–H in methyl and methylene groups which elucidated peaks at 1420 and 1363 cm^{-1}, attributed to the vibration of aliphatic C–H bonds (Veiga et al. 2020). The peak at 2356 cm^{-1} evidences the presence of the triple bond C≡C. The stretching

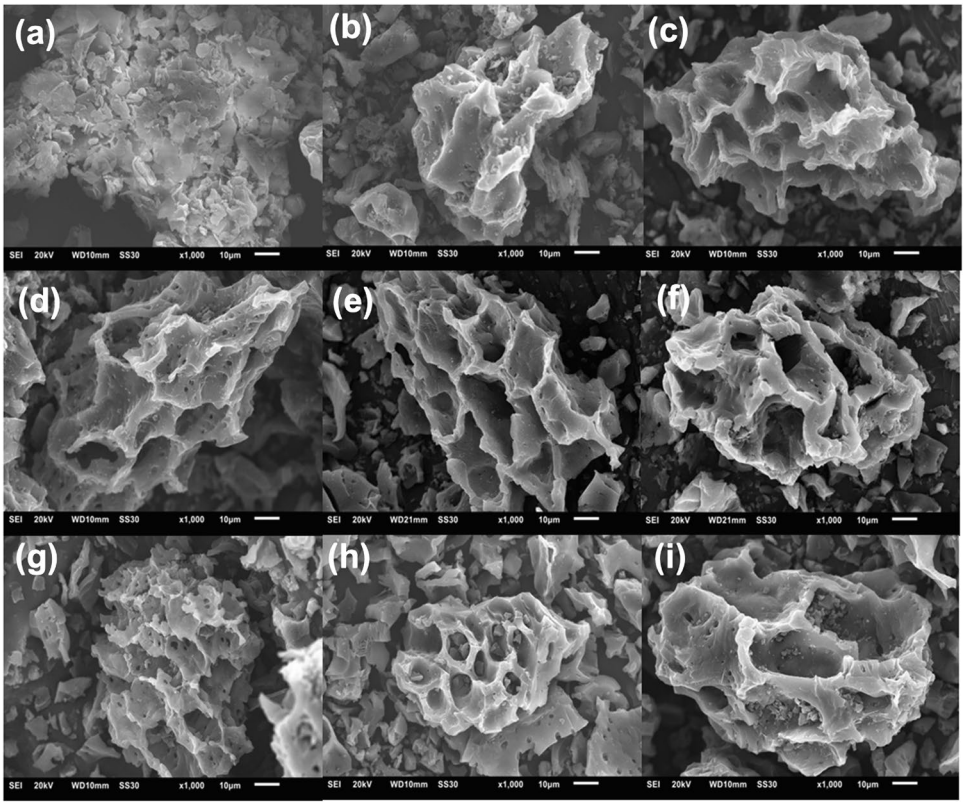

Fig. 2 SEM images of **a** ESS, **b** BC-400, **c** BC-500, **d** BC-600, **e** BC-700, **f** BC-800 °C, and BC-800 after adsorption of **g** IBP, **h** CAF, and **i** IBP

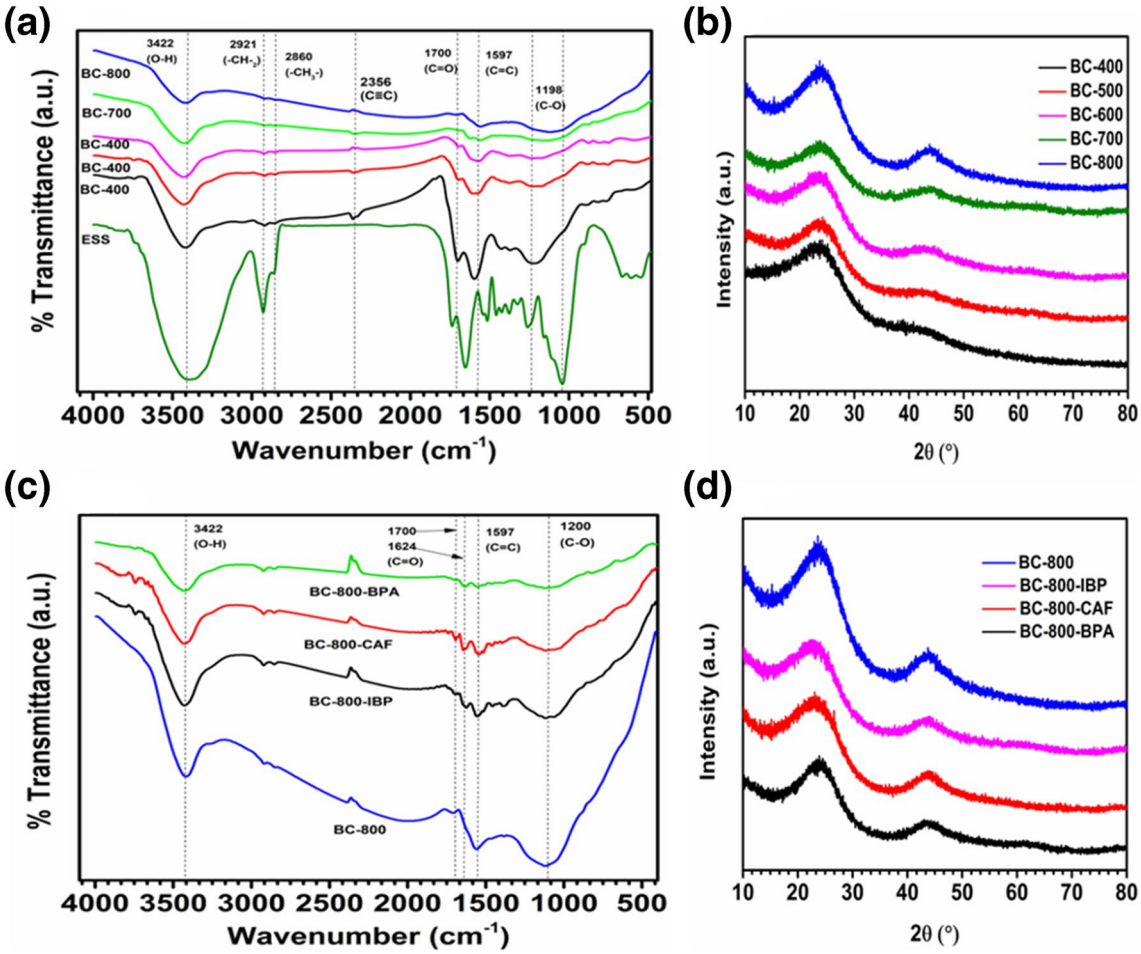

Fig. 3 FTIR spectra of **a** raw ESS and biochars and **c** BC-800 after adsorption of CECs; PXRD pattern of **b** biochars and **d** BC-800 after CEC adsorption

of carbonyl bond C = O is represented by the peak at 1700 cm^{-1} suggesting the presence of carboxylic and/or ketone functions on the surface of biochars. The peaks at 1597 and 1198 cm^{-1} are attributed to C = C and C–O respectively (Lekene et al. 2021). The almost total disappearance of peaks at 2921, 2890, 1420, and 1363 cm^{-1} on BC-700 and BC-800 indicates that the increase of the pyrolysis temperature accelerates the dehydrogenation which corroborates the results of elemental analysis.

As seen in Table 2 and Fig. S4, the pH of the solution at which the surface of the material is neutral (pH_{pzc}) gradually increases from 5.3 to 7.3 as the temperature increases from 400 to 800. At 400 °C, pH_{pzc} is less than 7 indicating an acidic surface while from 500 to 800 °C, the surface is almost neutral. At high temperatures, most of the oxygen-containing groups have been released. As known in the literature, the more oxygen the organic material contains, the more acidic is its surface (Boehm 1966). These results are consistent with the observations made by FTIR on the reduction of the intensity of some oxygen-containing groups.

The PXRD technique was used to assess the crystallinity of the biochars before and after adsorption. The PXRD patterns of the biochar samples portrayed in Fig. 3b show the absence of sharp reflection traducing the amorphous nature of prepared biochars. As expected, the broad diffraction reflection displayed by all the samples and centered at approximately $2\theta = 24°$ is indexed as the reflection from the (002) plane and is attributed to the characteristics of amorphous carbon material consisting of disordered polycyclic aromatic carbon sheets (Morales et al. 2021). At approximately 44° 2θ value, there is a new peak assigned to the diffraction of the (101) plane for graphitic and hexagonal carbons (Yan et al. 2021). The latter starts appearing on the sample BC-500 and becomes more prominent in BC-800. The observation of this new peak indicates the formation of a graphite-like structure as the pyrolysis temperature became higher. This graphitization of BC obtained at high temperature is the result of successive condensation reorganization of carbon atoms into aromatic rings, therefore leading to more stable and highly crystallized carbonaceous material

(Chaves Fernandes et al. 2020). In addition, the graphene layer of biochar has a significant influence on the adsorption of the targeted pollutants since it can interact with the π-electrons of the aromatic rings of CECs and enhance the adsorption process (Turk Sekulic et al. 2019).

Adsorption studies

Effect of pyrolysis temperature on the uptake of pollutants

Figure 4a shows the adsorption capacities of the biochars obtained at different pyrolysis temperatures. It can be observed that BC-800 has the highest removal efficiency toward IBP, CAF, and BPA with the maximum adsorbed quantities (removal percentage) of ~ 20 mg/g (64%), ~ 28 mg/g (95%), and ~ 27 mg/g (92%) respectively. The general trend is that, as the pyrolysis temperature increases from 400 to 800 °C, the adsorption performance increases. These results of the adsorption of CECs are consistent with the results of nitrogen adsorption leading to a strong symmetrical correlation between the specific surface area, pore volume, and maximum adsorption capacity. The removal of CECs mainly depends on the textural properties of the adsorbent, in agreement with results obtained by Tang et al. (2022) and Veiga et al. (2020) who prepared biochars from wheat straw and elephant grass for respective adsorption of bisphenol A and antibiotic and crystal violet dye. Based on its higher adsorption capacity compared to the other

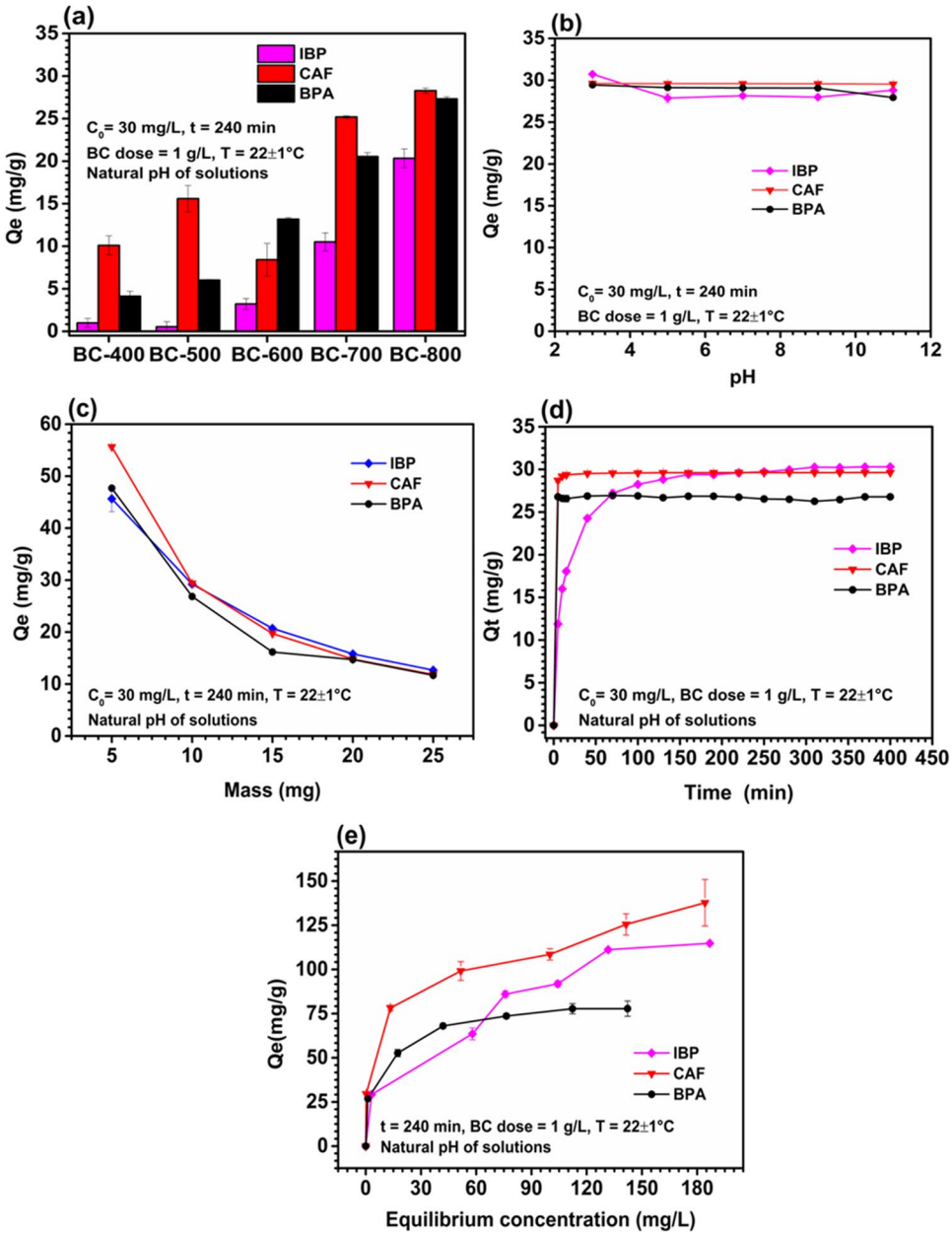

Fig. 4 **a** Adsorption capacity of CECs onto biochar prepared at different temperatures; effect of **b** pH, **c** mass, **d** contact time, and **e** initial concentration (adsorption isotherm), on the adsorption of CECs onto BC-800

biochars prepared at lower temperatures, BC-800 was subsequently selected for further experimental studies of the removal CECs from water.

Effect of pH

The pH is an important parameter affecting the adsorption capacity of compounds onto adsorbent materials since it influences the charge of the surface functional groups and may affect the ionization of the targeted pollutants. The amphoteric nature of biochar governing the changing of its charge surface strongly depends on the pH of the solution and the pH_{pzc} of biochar. The value of pH_{pzc} of BC-800 was found to be 7.35. At $pH > pH_{pzc}$, the surface charge of biochar is predominantly negative while at $pH < pH_{pzc}$, it is positive. The three CECs have pK_a values ranging between 5.2 and 14.0 as follows: IBP, 5.2; BPA, 9.6; and CAF, 14.0. Within the studied solution pH values (3–11), CAF remains uncharged compared to IBP and BPA, thus excluding the possibility to have an electrostatic interaction between CAF and biochar. Figure 4b shows IBP, CAF, and BPA adsorption capacity onto BC-800. It was evident that, within the studied range, no significant difference in the adsorption capacity of all CECs onto BC-800 at different pH levels was found. Similar results were reported in the literature (Tran et al. 2020; González-Hourcade et al. 2022; Correa-Navarro et al. 2022). This low pH dependence indicates that the adsorption mechanism of CECs onto BC-800 should not be mainly attributed to the electrostatic interactions but rather to other interactions such as pore filling with π-π interaction, hydrogen bonding, van der Waals interaction, and *n*-π interaction (Tran et al. 2017a; González-Hourcade et al. 2022). The selected biochar exhibits an excellent adsorption capacity for CECs under different pH values. Based on these observations, it was decided to conduct all further adsorption experiments at the natural pH of the solutions, that is, IBP 6.37, CAF 6.46, and BPA 7.05.

Effect of adsorbent dose

The effect of biochar dosage on the amount of CECs adsorbed was investigated by contacting 10 mL of CECs with different amounts of adsorbent varying in the range of 5–25 mg, keeping all the other parameters constant. The results depicted in Fig. 4c showed that the curves behaved in the same way for all three pollutants. The specific uptake of CECs decreases with the increasing mass of adsorbent as shown by Eq. (2). At high amounts of biochar, the available CECs in solution are not enough to cover all the vacant sites present on the adsorbent resulting in low adsorption capacity. Moreover, the reduction of the adsorbed quantity may also be due to the agglomeration of biochar particles at higher masses, limiting access to the adsorption sites available for CEC present in the solution due to the shielding effect which increases the diffusional path length (Suzaimi et al. 2019). On the other hand, because the initial concentration of pollutants remains unchanged and the adsorbed quantity does not increase proportionally with the increase in BC-800 mass, the adsorption capacity is reduced (González-Hourcade et al. 2022; Njewa et al. 2022).

Adsorption kinetics studies

The effect of contact time on IBP, CAF, and BPA adsorption on BC-800 was studied in the range of 5 to 400 min and is shown in Fig. 4d. It can be observed that as the contact time is increased, the rate of IBP adsorption gradually rises, and the equilibrium is established at around 160 min when the surface of biochar became saturated. For CAF and BPA, the kinetics of adsorption in the initial stage was rather faster than that of IBP with an equilibrium time of 40 min and only 5 min, respectively. In general, in the present work, just after 5 min, approximately 37, 96, and 95% of IBP, CAF, and BPA, respectively, present in the solution are adsorbed. The rapidity of the adsorption phenomenon which is similar to reported works (Karunanayake et al. 2017; Zbair et al. 2020; Liyanage et al. 2020) shows that the prepared biochar possesses high affinities with the targeted molecules in the solutions. Although the adsorption equilibrium was rapidly reached, to ensure its veracity, further experiments were conducted up to 400 min.

Four adsorption kinetics models including pseudo-first order, pseudo-second order, Elovich, and intraparticle diffusion presented in Table S3 were applied to mathematically describe the adsorption constants. The fitting curves and the relevant calculated parameters of all kinetic models are provided in Fig. 5a–c and Table 3 respectively. Based on the higher values of R^2 and the lower values of RMSE and χ^2, the pseudo-second-order model (0.99, 0.43, and 0.20) and Elovich model (0.99, 0.70, and 0.89) better describe the kinetic data of the adsorption of IBP than pseudo-first-order model (0.98, 1.19 and 2.26). Moreover, the value of $q_{e(\mathrm{cal})}$ calculated from the pseudo-second-order model was closer to the experimental value $q_{e(\mathrm{exp})}$. For the adsorption of CAF and BPA, the three kinetic models fitted the adsorption data well. Indeed, the values of R^2 were all higher than 0.99 along with very low values of error functions (RMSE and χ^2) as seen in Table 3. In addition, the adsorbed quantities ($q_{e(\mathrm{exp})}$) of CAF and BPA calculated from pseudo-first- and pseudo-second-order were all equal to the experimental values ($q_{e(\mathrm{cal})}$) respectively. α, the initial rate constant of the Elovich model (Table 3) for CAF and BPA, was higher than that for IBP suggesting that the prepared biochar exhibited a higher affinity towards the former CECs than the latter when the reaction began. It is well-known that the pseudo-first

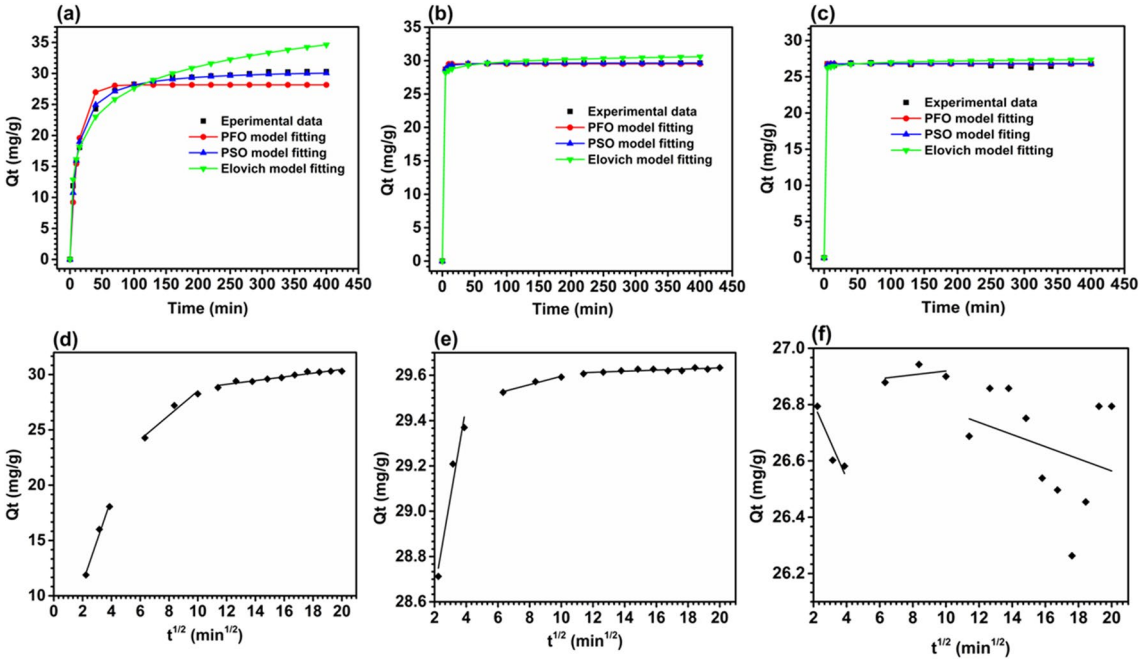

Fig. 5 Pseudo-first-order, pseudo-second-order, and Elovich kinetic model for adsorption of **a** IBP, **b** CAF, and **c** BPA and intraparticle diffusion fitting model for adsorption of **d** IBP, **e** CAF, and **f** BPA

and pseudo-second models suggest physical and chemical sorption respectively (Putra et al. 2009); moreover, the initial rate constant (α) is higher than the desorption constant (β) of the Elovich model; this demonstrates that the chemical reaction is occurring on the heterogeneous surface of biochar (Keerthanan et al. 2020).

The Weber and Morris intraparticle diffusion model was used to assess the steps governing the CEC removal and check the presence of diffusion mechanisms during the adsorption process on biochar. The plot of q_t versus $t^{1/2}$ (Fig. 5d–f) shows three straight lines with different slope and intercept values proving that during the adsorption of CECs onto biochar, different mechanisms, including bulk diffusion, intraparticle diffusion, and finally, adsorption at active sites, were involved (Mutavdžić Pavlović et al. 2021). Particularly for IBP and CAF, the values of the rate constants (k_{id}) and the constant (c) describe the thickness of the boundary layer following the order $k_{id1} > k_{id2} > k_{id3}$ and $c_1 < c_2 < c_3$ respectively (Table 3). These observations indicate that the adsorption rate gradually decreases while the effect on the limiting boundary layer gradually increases during the adsorption process indicating that the intraparticle diffusion stage is not the only rate-limiting step for the entire process. The adsorption rate may also be affected by chemical forces like H-bonding (Feng Feng et al. 2017; Wang and Zhang 2020). The intraparticle diffusion model did not fit well the experimental data of BPA adsorption due to the poor values of k_{id} and R^2 (Table 4).

Adsorption isotherm studies

The isotherms of CEC adsorption onto BC-800 obtained by plotting the adsorbed quantity (q_e) against equilibrium concentration (c_e) of each CECs (Fig. 4e) were all found to be L-type according to the Giles classification (Giles et al. 1974). The amounts of CECs adsorbed increased when increasing the initial concentration until the number of adsorption sites on the biochar became limited, leading to the competition between CEC molecules remaining in solution for the available sites. This type of isotherm indicates that the adsorption of CECs occurs due to relatively weak forces, such as van der Waals forces (Giles et al. 1974).

In the present work, to describe the adsorptive behavior of isotherm of CECs onto BC-800, four isotherm models (Table 4), two with two parameters (Langmuir and Freundlich), and two with three parameters (Redlich-Peterson and Sips) were used to describe the equilibrium data. The plots of the adsorption isotherm are shown in Fig. 6 while the derived parameters and error functions are given in Table 4. For the Langmuir isotherm, the value of separation factors (R_L) lies between 0 and 1 indicating that the adsorption process of all CECs onto the biochar was favorable (Gómez-Serrano et al. 2021). This observation can also be confirmed by the Freundlich model fitting results according to the values of $n > 1$ which indicate the favorability of the adsorption (Abuzalat et al. 2022). The Freundlich model fitted the experimental data better than

Table 3 Pseudo-first-order, pseudo-second-order, Elovich, and intraparticle kinetic fitting parameters for IBP, CAF, and BPA adsorption by BC-800

	Unit	IBP	CAF	BPA
$q_{e(\exp)}$	(mg/g)	29	30	27
Pseudo-first-order model				
$q_{e(\mathrm{cal})}$	(mg/g)	28	30	27
k_1	(min^{-1})	0.08	0.72	1.76
R^2	/	0.98	0.99	0.99
RMSE	/	1.19	0.10	0.10
χ^2	/	2.26	0.00	0.03
Pseudo-second-order model				
$q_{e(\mathrm{cal})}$	(mg/g)	31	30	30
K_2	($\mathrm{mg{\bullet}g^{-1}{\bullet}min^{-1}}$)	0.004	0.21	1.31
R^2	/	0.99	0.99	0.99
RMSE	/	0.43	0.01	0.09
χ^2	/	0.20	0.00	0.03
Elovich model				
α	($\mathrm{mg{\bullet}g^{-1}{\bullet}min^{-1}}$)	11.80	1.2E+21	1.2E+41
β	($\mathrm{g{\bullet}min^{-1}}$)	0.20	1.80	3.72
R^2	/	0.99	0.99	0.99
RMSE	/	0.70	0.35	0.23
χ^2	/	0.89	0.11	0.08
Intraparticular diffusion model				
Stage 1				
k_{id1}	($\mathrm{mg{\bullet}g^{-1}{\bullet}min^{-1/2}}$)	3.81	0.41	−0.13
c_1	($\mathrm{mg{\bullet}g^{-1}}$)	4	28	27
R^2	/	0.99	0.96	0.88
Stage 2				
k_{id2}	($\mathrm{mg{\bullet}g^{-1}{\bullet}min^{-1/2}}$)	0.89	0.02	0.01
c_2	($\mathrm{mg{\bullet}g^{-1}}$)	19	29	28
R^2	/	0.93	0.98	0.15
Stage3				
k_{id3}	($\mathrm{mg{\bullet}g^{-1}{\bullet}min^{-1/2}}$)	0.15	0.01	-0.02
c_3	($\mathrm{mg{\bullet}g^{-1}}$)	27	30	27
R^2	/	0.93	0.69	0.09

Table 4 Langmuir, Freundlich, Temkin, and Sips isotherm adsorption parameters for (a) IBP, (b) CAF, and BPA adsorption by BC-800

	Unit	IBP	CAF	BPA
Langmuir model				
q_m	$\mathrm{mg{\bullet}g^{-1}}$	180	121	73
K_L	$\mathrm{L{\bullet}mg^{-1}}$	0.01	0.14	0.37
R_L		0.75–0.29	0.19–0.02	0.08–0.01
R^2		0.93	0.93	0.96
RMSE		11.24	13.19	6.18
χ^2		86.71	221.07	4.21
Freundlich model				
K_F	($\mathrm{L{\bullet}g^{-1}}$)	13.54	43.83	27.85
n		2.39	4.83	4.47
R^2		0.98	0.99	0.99
RMSE		7.50	3.58	2.38
χ^2		4.76	1.15	0.92
Sips model				
q_{mS}	$\mathrm{mg{\bullet}g^{-1}}$	219,629	595	118
K_S	$\mathrm{L{\bullet}g^{-1}}$	7E−5	0.08	0.27
n_S		0.39	0.25	0.41
R^2		0.99	0.99	0.99
RMSE		7.77	5.32	2.01
χ^2		3.60	1.00	0.26
Redlich-Peterson model				
K_{RP}	L/g	0.85	1.00	0.04
α_{RP}	$\mathrm{L/mg^{-1}}$	0.08	0.06	20.62
β_{RP}		0.00	0.00	0.00
R^2		0.96	0.83	0.81
RMSE		17.13	48.38	30.69
χ^2		237.19	44,479.66	931.89

Langmuir according to the calculated error functions, (high values R^2 and low values RMSE and χ^2) indicating that the adsorption of the different CECs onto BC-800 tends to multilayer adsorption. Based on the values of R^2, RMSE, and χ^2 (Table 4), the Sips isotherm model was also found to be good for representing the equilibrium data as well as Freundlich isotherm, suggesting that the adsorption is taking place on a heterogeneous surface (Nanta et al. 2018). The Redlich-Peterson model was not suitable to represent the equilibrium adsorption data due to its lowest values of R^2 and very high values of RMSE and χ^2 (Table 4). Nevertheless, it found that for the three CECs, the values of the Redlich-Peterson and β_{RP} were all equal to zero indicating that the model represents the Henry law that approaches the Freundlich isotherm (Hua 2018). The error function values of the four studied models can be classified in a descending order as follows: Sips > Freundlich > Langmuir > Redlich-Peterson. The results revealed that a three-parameter model rather than the two-parameter model is needed to achieve a good fit of the equilibrium data.

The Langmuir monolayer adsorption capacity of the prepared biochar for IBP, CAF, and BPA was compared to some reported carbonaceous adsorbents in the literature (Table S4). It was found that BC-800 showed a higher CEC adsorption capacity ($q_{\max}$ = ~ 180, 121, and 73 mg/g for IBP, CAF, and BPA, respectively) compared to adsorbents like activated carbon, activated biochar, and magnetic activated carbon (seen Table S4). Thus, the prepared biochar from egusi seed shells, obtained by simple single-step pyrolysis, presents an interesting possibility to valorize these agricultural by-products for wastewater treatment.

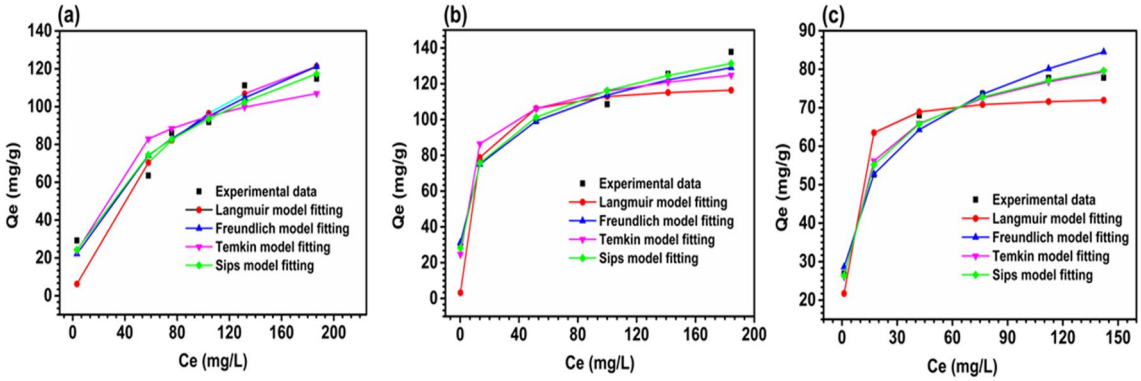

Fig. 6 Langmuir, Freundlich, Temkin, and Sips isotherm adsorption model for **a** IBP, **b** CAF, and BPA adsorption by BC-800

Table 5 Thermodynamic parameters of the adsorption of IBP, CAF, and BPA onto BC-800

Temperature (K)	van't Hoff equation	Thermodynamic parameters		
		$\Delta G°$ (kJ/mol)	$\Delta S°$ (kJ/mol.K) × 10^{-3}	$\Delta H°$ (kJ/mol)
IBP				
303	$y = -817.08x + 3.43$ ($R^2 = 0.99$)	−1.87		
313		−2.17	27.77	6.79
323		−2.44		
CAF				
303	$y = -1791.07x + 7.11$ ($R^2 = 0.91$)	−2.98		
313		−3.74	59.11	14.89
323		−4.15		
BPA				
303	$y = -559.71x + 2.35$ ($R^2 = 0.65$)	−1.24		
313		−1.55	19.54	4.65
323		−1.63		

Adsorption thermodynamics studies

In other to evaluate the feasibility and spontaneity of the adsorption process of different CECs onto BC-800, thermodynamic parameters such as free energy change ($\Delta G°$), enthalpy change ($\Delta H°$), and entropy change ($\Delta S°$) were calculated using the Gibbs free energy and van't Hoff equations (Table S3) and the plot of $\ln K_c$ vs. $1/T$ (Fig. S5). Table 5 lists the value of $\Delta G°$, $\Delta H°$, and $\Delta S°$ at three different temperatures (303, 313, and 323 K). The spontaneity and feasibility of the adsorption process are indicated by the negative value of $\Delta G°$, while the positive value of $\Delta S°$ indicates the increase in randomness and disorder of the adsorbent surface after adsorption. The positive value of $\Delta H°$ indicates that the adsorption process was endothermic (Kaya et al. 2021).

Desorption study

The desorption study of CECs is essential to understand the adsorption characteristics and also the adsorption mechanism. The percentage of desorption of CECs using different desorbing agents is given in Table 6. The obtained results indicate that the amount of CECs that could be desorbed was small for all desorbing agents that were tested. Nevertheless, the best but still poor desorption was achieved using ethanol and methanol for all CECs. The poor desorption could also be explained by the irreversibility of

Table 6 Desorption efficiency of CECs from the loaded BC-800 using various desorbing agents

Desorbing agent	Desorption efficiency (%)		
	IBP	CAF	BPA
Deionized water	8.66	0.23	1.26
Ethanol	14.62	6.08	9.08
NaCl (0.1 M)	5.50	0.35	1.12
Methanol	15.95	8.50	13.21
HCl (0.1 M)	2.24	0.27	7.48
NaOH (0.1 M)	6.30	0.19	1.97

the adsorption process of CECs onto BC-800 that can be related to the separation factor, R_L (Table 4). Indeed, when $0 < R_L < 1$, the adsorption is favorable and becomes increasingly irreversible when its value approaches zero (Hua 2018). A similar result was reported by Tran and collaborators (Tran et al. 2017a) for the regeneration of activated charcoal after the adsorption of methylene green dye using various desorbing agents. In addition, the trapping of the molecules inside the pores of biochar may also explain the poor desorption of CECs.

Adsorption mechanism

Due to the presence of various surface functional groups (i.e., – COOH, –OH, C = O) and benzene rings in carbonaceous materials, several mechanisms have been suggested for the removal of CECs from aqueous media including van der Waals forces, π-π and *n*-π interaction, electrostatic attraction, and hydrogen bonding (Tran et al. 2020; Keerthanan et al. 2020; Czech et al. 2021; Naima et al. 2022). The adsorption mechanism depends on the adsorbent properties (i.e., surface functional groups, surface area, and pore size distribution), adsorbate characteristics (i.e., solubility, molecular size, and pK_a), and strongly on the experimental adsorption conditions (i.e., temperature, initial concentration and pH). Therefore, in the present study, the adsorption mechanism of IBP, CAF, and BPA onto biochar BC-800 was investigated using a solution concentration of 100 mg/L without any pH adjustment, during 60 min at room temperature.

The study of the effect of pH on the adsorption of CECs shows that no significant effect of electrostatic attraction can be involved in the adsorption mechanism of CECs. The FTIR (Fig. 3c) spectra of BC-800 after adsorption of IBP, CAF, and BPA gave much information related to the type of interaction involved in the adsorption mechanism. The reduction in intensity of the band at 3422 cm^{-1} after adsorption of all the CECs suggests the formation of hydrogen bonding interaction. The hydrogen bonding can be regarded as dipole–dipole hydrogen bonding and Yoshida hydrogen bonding. The former is due to the interaction between –OH groups (H-donor) on BC-800 and the H-acceptor like nitrogen and oxygen while the latter is related to the interaction between –OH groups on BC-800 and aromatic rings in IBP, CAF, and BPA molecules (Tran et al. 2017b).

For the *n*-π electron donor–acceptor interactions also known as *n*-π interactions, reported for the first time by Mattson et al. (Mattson et al. 1969), the aromatic rings of CECs act as electron acceptors while a carbonyl group of BC acts as an electron donor. The observation of FTIR (Fig. 3c) of BC-800 before and after adsorption shows the reduction of the intensities of the peaks at 1200 cm^{-1} corresponding to C–O. In addition to the reduction of the intensity of the peak at 1700 cm^{-1} corresponding to C = O groups, it is shifted to a lower wavenumber (1624 cm^{-1}) thus indicating the intervention of *n*-π interactions in the adsorption mechanism which is consistent with reported works (Tran et al. 2017a, 2020; Turk Sekulic et al. 2019).

Between the π-electrons of biochar and the π-electrons of CECs, π-π interactions can occur which can be evidenced by the FTIR (Fig. 3c) analysis (Tran et al. 2017a; Turk Sekulic et al. 2019). Indeed, the intensity of the peak corresponding to aromatic C = C bonds (at 1597 cm^{-1}) in biochar decreases after adsorption indicating the presence of π-π interactions between the benzene rings of biochar and CECs. Similar results were obtained in the literature (Xu et al. 2012; Correa-Navarro et al. 2022).

The PXRDs show (Fig. 3d) no shifts after adsorption of the three CECs indicating that there were no occurrence of phase transformation. However, a significant change in the intensities was observed and could be attributed to the surface adsorption of CECs (Banerjee et al. 2016; Turk Sekulic et al. 2019). The adsorption process was mainly governed by physisorption.

The van der Waals forces can also be involved in the adsorption mechanism. It has been reported that the intensities of van der Waals forces of an adsorbed molecule are proportional to its contact surface area with the adsorbent. Moreover, the graphene surface of carbonaceous material has a high van der Waals index, and the IBP, CAF, and BPA molecules have a large planar ring structure; therefore, van der Waals forces can occur between the CEC molecules and the graphene-like surface of BC-800 (Ji et al. 2009).

N_2 sorption was also used to assess the adsorption mechanism of CECs on biochar since there is a close relationship between the pore properties of the adsorbent and the size of the adsorbate (Tran et al. 2017b). Figure 1e shows that the uptake of nitrogen adsorbed on CEC-loaded biochar (BC-800-IBP, BC-800-CAF, and BC-800-BPA) is remarkably lower than that of pristine biochar (BC-800), as expected. Pore filling of the CEC lowers both the still available surface area and pore volume for N_2 adsorption, possibly also together with pore blocking (see Table S5 and Fig. 1e, f). Several reported works revealed that pore filling was involved in the adsorption mechanism of pharmaceuticals such as ibuprofen (Naima et al. 2022), paracetamol (Tran et al. 2020), carbamazepine, naproxen, and diclofenac (Turk Sekulic et al. 2019) onto carbonaceous material.

There was no significant difference between SEM images of BC-800 before and after CEC adsorption (Fig. 2h-i) indicating that the adsorption took place in the inner pore surfaces (micro- and mesopores) which were not accessible by SEM. To sum up, the proposed mechanism of adsorption of CECs onto the prepared biochar which includes hydrogen bonding, van der Waals force, π-π and n-π interactions, and pore filling is schemed in Fig. 7.

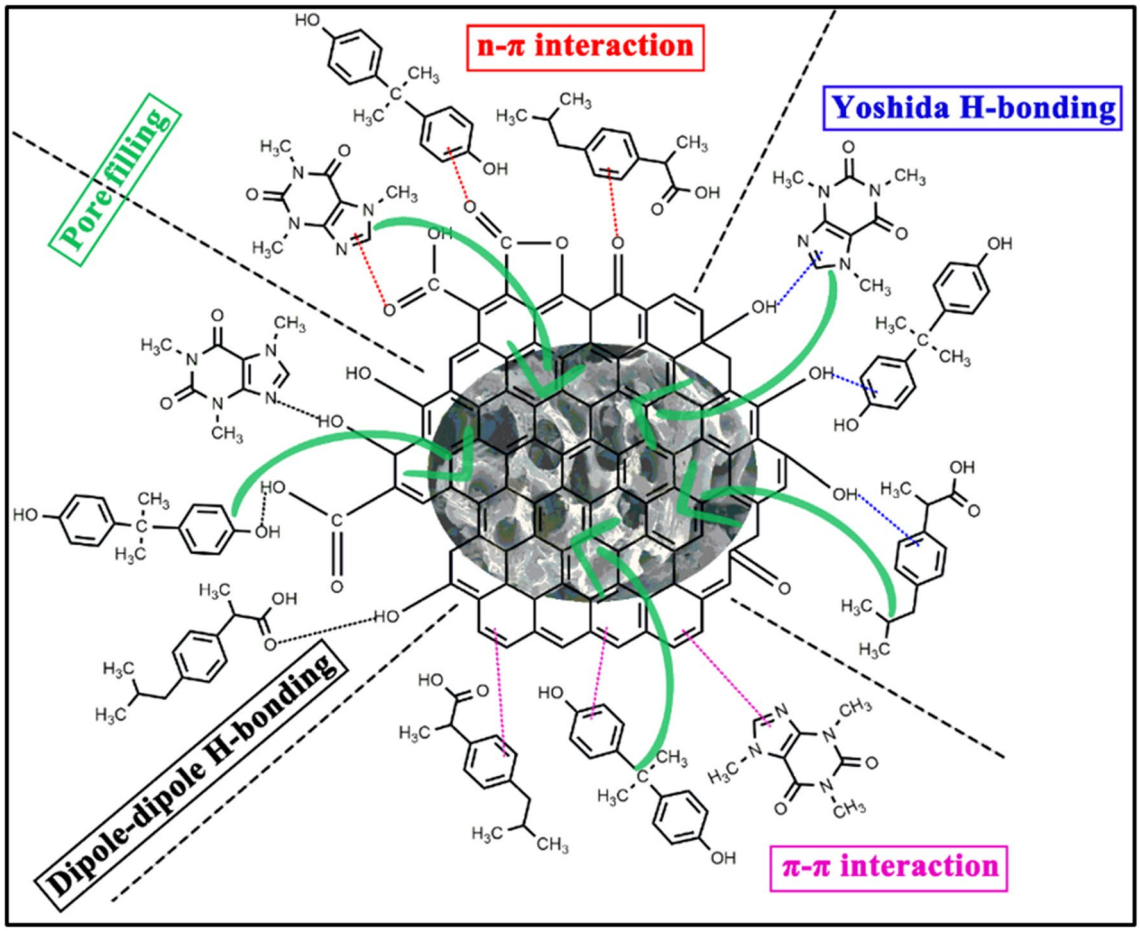

Fig. 7 Proposed mechanism of adsorption of CECs onto BC-800 from egusi seed shells

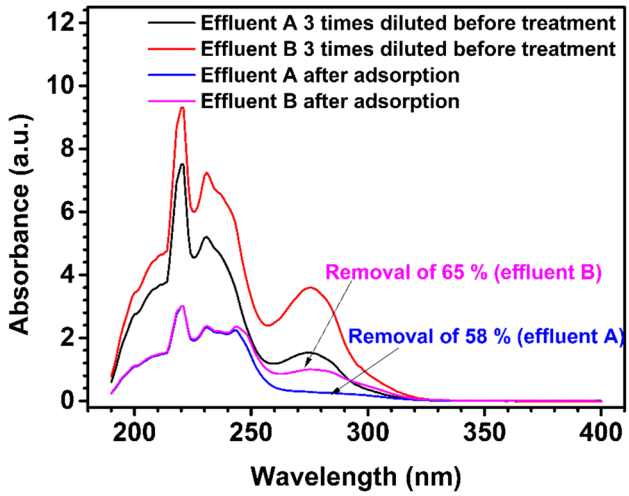

Fig. 8 UV–vis spectra of simulated pharmaceutical effluents before and after the adsorption using BC-800

Treatment of synthetic effluent

Based on the adsorption data, BC-800 shows good efficiency in the removal of IBP, CAF, and BPA from water in a single aqueous solution indicating that it could be suitable for the treatment of real wastewater. Therefore, two simulated hospital effluent samples with different chemical species including pharmaceuticals and organic and inorganic components (Table 1) were used to test the efficiency of BC-800 to clean them up (see Fig. 8). The removal percentage of compounds present in the effluents was assessed by integrating the surface area under the absorption band from 190 to 400 nm of treated effluent divided by the area under the absorption band of the untreated effluent (González-Hourcade et al. 2022; Cavalcante et al. 2022). The overall removal percentage was around 58

Table 7 Biochar production's cost estimation

Particular	Sub-sections	Cost break-up	Total cost (USD)
Raw material processing	Collection of raw materials for BC production	Egusi seed shells were collected from a local market for free	0.00
Preparation of BC	Pyrolysis process	Hours × power × unitcost = 2.33 × 1.8 × 0.16	0.67
	Drying process	Hours × power × unitcost = 36 × 0.75 × 0.16	4.32
Washing	Washing process	Deionized water used for washing was obtained from a laboratory set-up	0.00
			4.99

and 65% for effluent A and effluent B respectively. These results show that the BC-800 seems to be more efficient at high concentrations of pollutants which is consistent with the results of the study of the initial concentration. These results suggest that the biochar obtained using egusi seed shells as starting material can be used for practical applications.

Cost evaluation and economical-environmental analysis

Evaluating the production costs of an adsorbent is an important factor in other to evaluate its rentability at large-scale for wastewater treatment (Yang et al. 2022; Lekene et al. 2023). In the present study, the cost of producing biochar was evaluated, based on the cost of electricity in the production area (Cameroon). The raw material was collected free from a market in Yaoundé and the deionized water used for washing came from the laboratory facilities. Only the pyrolysis and drying stages were considered in this assessment of biochar production costs, as shown in Table 7. As the price of electricity in Cameroon is set at around USD 0.16 USD/kWh, the estimated cost for the production of 1 kg of biochar was found to be 4.99 USD. The main operational cost comes from the drying stage. This could be further reduced by sun drying of the raw material suggesting the potential in practical application of biochar-based egusi seed shells.

Conclusion

From this study, biochar with good physicochemical properties was successfully prepared and characterized from egusi seed shells and used for the removal of CECs from water. As the pyrolysis temperature increased from 400 to 800 °C, the BC yield, the H, N, and O content decreased while the BET surface area, total pore volume, and ash content increased. The SEM images showed that macroporous honeycomb-like structures are created at high temperatures. The biochar obtained at 800 °C displaying the highest specific surface area (688 m^2/g) possessed the best performance towards the elimination of CECs with the Langmuir maximum monolayer adsorption capacities of 180, 121, and 73 mg/g respectively for IBP, CAF, and BPA. The kinetic data were better described by pseudo-second-order and Elovich model while Sips and Freundlich isotherm models were used to better fit of the equilibrium data. The thermodynamic study shows that the adsorption process was spontaneous and endothermic for the three CECs. FTIR, PXRD, SEM, and BET analyses show that the adsorption mechanism of CECs was supported by hydrogen bonding, van der Waals force, π-π, and n-π interactions. The pore filling was also found to be one of the most important contributors to the adsorption mechanism. Due to its high adsorption capacities and good textural properties, the prepared biochar is a promising adsorbent for wastewater treatment.

Supplementary Information The online version contains supplementary material available at https://doi.org/10.1007/s11356-023-29377-w.

Acknowledgements The authors thank Mrs. Birgit Tommes for the FTIR analysis.

Author contribution All authors contributed to the study's conception and design. René Blaise Ngouateu Lekene: conceptualization ideas, methodology, investigation, writing original draft, and funding acquisition; Tobie Matemb Ma Ntep: writing, review, and editing; Marcus N. A. Fetzer and Till Strothmann: resources; Julius Ndi Nsami: resources and validation; Christoph Janiak: supervision, writing, review, editing, project administrator, and funding acquisition.

Funding This research was supported by the German Academic Exchange Service (DAAD) under the Research Grants-Short-Term scholarship program (grant number: 91831392) and the African-German Network of Excellence in Science (AGNES) Grant for Juniors Researchers in collaboration with the Alexander von Humboldt Foundation (AvH) and the German Ministry of Education and Research (BMBF), 2022.

Data availability All data and materials are available upon reasonable request.

Declarations

Ethical approval Not applicable.

Consent to participate Not applicable.

Consent for publication All the authors consent to publication.

Competing interests The authors declare no competing interests.

References

Abuwatfa WH, Al-Muqbel D, Al-Othman A et al (2021) Insights into the removal of microplastics from water using biochar in the era of COVID-19: a mini review. Case Stud Chem Environ Eng 4:100151. https://doi.org/10.1016/j.cscee.2021.100151

Abuzalat O, Wong D, Elsayed MA (2022) Nano-porous composites of activated carbon–metal organic frameworks (Fe-BDC@AC) for rapid removal of Cr (VI): synthesis, adsorption, mechanism, and kinetics studies. J Inorg Organomet Polym 32:1924–1934. https://doi.org/10.1007/s10904-022-02237-9

Acero JL, Benitez FJ, Real FJ, Rodriguez E (2015) Elimination of selected emerging contaminants by the combination of membrane filtration and chemical oxidation processes. Water Air Soil Pollut 226:139. https://doi.org/10.1007/s11270-015-2404-8

Antero RVP, Alves ACF, de T Ferreira Sales P et al (2019) A new approach to obtain mesoporous-activated carbon via hydrothermal carbonization of Brazilian Cerrado biomass combined with physical activation for bisphenol-A removal. Chem Eng Commun 206:1498–1514. https://doi.org/10.1080/00986445.2019.1601625

Arman NZ, Salmiati S, Aris A et al (2021) A review on emerging pollutants in the water environment: existences, health effects and treatment processes. Water 13:3258. https://doi.org/10.3390/w13223258

Banerjee S, Sharma GC, Gautam RK et al (2016) Removal of Malachite Green, a hazardous dye from aqueous solutions using Avena sativa (oat) hull as a potential adsorbent. J Mol Liq 213:162–172. https://doi.org/10.1016/j.molliq.2015.11.011

Barrios JA, Cano A, Becerril JE, Jiménez B (2016) Influence of solids on the removal of emerging pollutants in electrooxidation of municipal sludge with boron-doped diamond electrodes. J Electroanal Chem 776:148–151. https://doi.org/10.1016/j.jelechem.2016.07.018

Boehm HP (1966) Chemical identification of surface groups. In: Eley DD, Pines H, Weisz PB (eds) Advances in catalysis. Academic Press, pp 179–274

Cavalcante EHM, Candido ICM, de Oliveira HP et al (2022) 3-Aminopropyl-triethoxysilane-functionalized tannin-rich grape biomass for the adsorption of methyl orange dye: synthesis, characterization, and the adsorption mechanism. ACS Omega 7:18997–19009. https://doi.org/10.1021/acsomega.2c02101

Chaves Fernandes BC, Ferreira Mendes K, Dias Júnior AF et al (2020) Impact of pyrolysis temperature on the properties of eucalyptus wood-derived biochar. Materials 13:5841. https://doi.org/10.3390/ma13245841

Cheng N, Wang B, Wu P et al (2021) Adsorption of emerging contaminants from water and wastewater by modified biochar: a review. Environ Pollut 273:116448. https://doi.org/10.1016/j.envpol.2021.116448

Correa-Navarro YM, Moreno-Piraján JC, Giraldo L (2022) Processing of fique bagasse waste into modified biochars for adsorption of caffeine and sodium diclofenac. Braz J Chem Eng 39:933–948. https://doi.org/10.1007/s43153-021-00191-6

Czech B, Kończak M, Rakowska M, Oleszczuk P (2021) Engineered biochars from organic wastes for the adsorption of diclofenac, naproxen and triclosan from water systems. J Clean Prod 288:125686. https://doi.org/10.1016/j.jclepro.2020.125686

Elnour AY, Alghyamah AA, Shaikh HM et al (2019) Effect of pyrolysis temperature on biochar microstructural evolution, physicochemical characteristics, and its influence on biochar/polypropylene composites. Appl Sci 9:1149. https://doi.org/10.3390/app9061149

Feng Feng M, BaoWei Z, JingRu D (2017) Adsorptive characteristics of cadmium onto biochar produced from pyrolysis of wheat straw in aqueous solution. China Environ Sci 37:551–559

Ferreira L, Rosales E, Danko AS et al (2016) Bacillus thuringiensis a promising bacterium for degrading emerging pollutants. Process Saf Environ Prot 101:19–26. https://doi.org/10.1016/j.psep.2015.05.003

Galindo-Miranda JM, Guízar-González C, Becerril-Bravo EJ et al (2019) Occurrence of emerging contaminants in environmental surface waters and their analytical methodology – a review. Water Supply 19:1871–1884. https://doi.org/10.2166/ws.2019.087

Giles CH, Smith D, Huitson A (1974) A general treatment and classification of the solute adsorption isotherm. I. Theoretical. J Colloid Interface Sci 47:755–765. https://doi.org/10.1016/0021-9797(74)90252-5

Gogoi A, Mazumder P, Tyagi VK et al (2018) Occurrence and fate of emerging contaminants in water environment: a review. Groundw Sustain Dev 6:169–180. https://doi.org/10.1016/j.gsd.2017.12.009

Gómez-Serrano V, Adame-Pereira M, Alexandre-Franco M, Fernández-González C (2021) Adsorption of bisphenol A by activated carbon developed from PET waste by KOH activation. Environ Sci Pollut Res 28:24342–24354. https://doi.org/10.1007/s11356-020-08428-6

González-Hourcade M, Simões dos Reis G, Grimm A et al (2022) Microalgae biomass as a sustainable precursor to produce nitrogen-doped biochar for efficient removal of emerging pollutants from aqueous media. J Clean Prod 348:131280. https://doi.org/10.1016/j.jclepro.2022.131280

Gurav R, Bhatia SK, Choi T-R et al (2022) Adsorptive removal of synthetic plastic components bisphenol-A and solvent black-3 dye from single and binary solutions using pristine pinecone biochar. Chemosphere 296:134034. https://doi.org/10.1016/j.chemosphere.2022.134034

Hadj-Otmane Ch, Ouakouak A, Touahra F et al (2022) Date palm petiole–derived biochar: effect of pyrolysis temperature and adsorption properties of hazardous cationic dye from water. Biomass Conv Bioref. https://doi.org/10.1007/s13399-022-03127-3

Hua J (2018) Adsorption of low-concentration arsenic from water by co-modified bentonite with manganese oxides and poly(dimethyldiallylammonium chloride). J Environ Chem Eng 6:156–168. https://doi.org/10.1016/j.jece.2017.11.062

Hung C-Y, Tsai W-T, Chen J-W et al (2017) Characterization of biochar prepared from biogas digestate. Waste Manage 66:53–60. https://doi.org/10.1016/j.wasman.2017.04.034

Jha S, Gaur R, Shahabuddin S, Tyagi I (2023) Biochar as sustainable alternative and green adsorbent for the remediation of noxious pollutants: a comprehensive review. Toxics 11:117. https://doi.org/10.3390/toxics11020117

Ji L, Chen W, Duan L, Zhu D (2009) Mechanisms for strong adsorption of tetracycline to carbon nanotubes: a comparative study using activated carbon and graphite as adsorbents. Environ Sci Technol 43:2322–2327. https://doi.org/10.1021/es803268b

Ji Y, Zheng N, An Q et al (2022) The effect of carbonization temperature on the capacity and mechanisms of Cd(II)-Pb(II) mix-ions adsorption by wood ear mushroom sticks derived biochar. Ecotoxicol Environ Saf 239:113646. https://doi.org/10.1016/j.ecoenv.2022.113646

Karunanayake AG, Todd OA, Crowley ML et al (2017) Rapid removal of salicylic acid, 4-nitroaniline, benzoic acid and phthalic acid from wastewater using magnetized fast pyrolysis biochar from waste Douglas fir. Chem Eng J 319:75–88. https://doi.org/10.1016/j.cej.2017.02.116

Kaya N, Yıldız Uzun Z, Altuncan C, Uzun H (2021) Adsorption of Congo red from aqueous solution onto KOH-activated biochar produced via pyrolysis of pine cone and modeling of the process using artificial neural network. Biomass Conv Bioref. https://doi.org/10.1007/s13399-021-01856-5

Keerthanan S, Bhatnagar A, Mahatantila K et al (2020) Engineered tea-waste biochar for the removal of caffeine, a model compound in pharmaceuticals and personal care products (PPCPs), from aqueous media. Environ Technol Innov 19:100847. https://doi.org/10.1016/j.eti.2020.100847

Kozyatnyk I, Oesterle P, Wurzer C et al (2021) Removal of contaminants of emerging concern from multicomponent systems using carbon dioxide activated biochar from lignocellulosic feedstocks. Bioresource Technol 340:125561. https://doi.org/10.1016/j.biortech.2021.125561

Lékéné RBN, Nsami JN, Rauf A et al (2018) Optimization conditions of the preparation of activated carbon based egusi (*Cucumeropsis mannii* Naudin) seed shells for nitrate ions removal from wastewater. Am J Anal Chem 09:439. https://doi.org/10.4236/ajac.2018.910034

Lekene RBN, Kouotou D, Ankoro NO et al (2021) Development and tailoring of amino-functionalized activated carbon based Cucumerupsi manni Naudin seed shells for the removal of nitrate ions from aqueous solution. J Saudi Chem Soc 25:101316. https://doi.org/10.1016/j.jscs.2021.101316

Lekene RBN, Ankoro NO, Kouotou D et al (2023) High-quality low-cost activated carbon/chitosan biocomposite for effective removal of nitrate ions from aqueous solution: isotherm and kinetics studies. Biomass Conv Bioref. https://doi.org/10.1007/s13399-023-04239-0

Li L, Zou D, Xiao Z et al (2019) Biochar as a sorbent for emerging contaminants enables improvements in waste management and sustainable resource use. J Clean Prod 210:1324–1342. https://doi.org/10.1016/j.jclepro.2018.11.087

Liao J, Chen H, Zhang Y, Zhu W (2022) Pyrolysis of animal manure under nitrogen atmosphere: an environment protection way to obtain animal manure biochar for high-efficient adsorption of uranium (VI). J Anal Appl Pyrol 163:105493. https://doi.org/10.1016/j.jaap.2022.105493

Lima DR, Hosseini-Bandegharaei A, Thue PS et al (2019) Efficient acetaminophen removal from water and hospital effluents treatment by activated carbons derived from Brazil nutshells. Colloids Surf A: Physicochem Eng Asp 583:123966. https://doi.org/10.1016/j.colsurfa.2019.123966

Liyanage AS, Canaday S, Pittman CU, Mlsna T (2020) Rapid remediation of pharmaceuticals from wastewater using magnetic Fe3O4/Douglas fir biochar adsorbents. Chemosphere 258:127336. https://doi.org/10.1016/j.chemosphere.2020.127336

Mattson JA, Mark HB, Malbin MD et al (1969) Surface chemistry of active carbon: specific adsorption of phenols. J Colloid Interface Sci 31:116–130. https://doi.org/10.1016/0021-9797(69)90089-7

Maziarka P, Sommersacher P, Wang X et al (2021) Tailoring of the pore structures of wood pyrolysis chars for potential use in energy storage applications. Applied Energy 286:116431. https://doi.org/10.1016/j.apenergy.2020.116431

Morales LF, Herrera K, López JE, Saldarriaga JF (2021) Use of biochar from rice husk pyrolysis: assessment of reactivity in lime pastes. Heliyon 7:e08423. https://doi.org/10.1016/j.heliyon.2021.e08423

Mutavdžić Pavlović D, Ćurković L, Mandić V et al (2021) Removal of pharmaceuticals from water by tomato waste as novel promising biosorbent: equilibrium, kinetics, and thermodynamics. Sustainability 13:11560. https://doi.org/10.3390/su132111560

Naima A, Ammar F, Abdelkader O et al (2022) Development of a novel and efficient biochar produced from pepper stem for effective ibuprofen removal. Bioresource Technol 347:126685. https://doi.org/10.1016/j.biortech.2022.126685

Nanta P, Kasemwong K, Skolpap W (2018) Isotherm and kinetic modeling on superparamagnetic nanoparticles adsorption of polysaccharide. J Environ Chem Eng 6:794–802. https://doi.org/10.1016/j.jece.2017.12.063

Njewa JB, Biswick TT, Vunain E et al (2022) Synthesis and characterization of activated carbon from agrowastes for the removal of acetic acid from an aqueous solution. Adsorpt Sci Technol 2022:e7701128. https://doi.org/10.1155/2022/7701128

Oginni O, Singh K (2021) Effect of carbonization temperature on fuel and caffeine adsorption characteristics of white pine and Norway spruce needle derived biochars. Ind Crop Prod 162:113261. https://doi.org/10.1016/j.indcrop.2021.113261

Osman AI, Fawzy S, Farghali M et al (2022) Biochar for agronomy, animal farming, anaerobic digestion, composting, water treatment, soil remediation, construction, energy storage, and carbon sequestration: a review. Environ Chem Lett 20:2385–2485. https://doi.org/10.1007/s10311-022-01424-x

Popoola LT, Yusuff AS, Ikumapayi OM et al (2022) Electrochemical, isotherm, and material strength studies of *Cucumeropsis mannii* shell extract on A515 grade 70 carbon steel in NaCl solution. Int J Corros 2022:e3189844. https://doi.org/10.1155/2022/3189844

Putra EK, Pranowo R, Sunarso J et al (2009) Performance of activated carbon and bentonite for adsorption of amoxicillin from wastewater: mechanisms, isotherms and kinetics. Water Res 43:2419–2430. https://doi.org/10.1016/j.watres.2009.02.039

Sahoo S, Vijay V, Chandra R, Kumar H (2021) Production and characterization of biochar produced from slow pyrolysis of pigeon pea stalk and bamboo. Clean Eng Technol. https://doi.org/10.1016/J.CLET.2021.100101

Siara S, Elvis C, Harishkumar R, Velayudhaperumal Chellam P (2022) ZnAl2O4 supported on lychee-biochar applied to ibuprofen photodegradation. Mater Res Bull 145:111530. https://doi.org/10.1016/j.materresbull.2021.111530

Souza HdeO, dos S Costa R, Quadra GR, dos S Fernandez MA (2021) Pharmaceutical pollution and sustainable development goals: going the right way? Sustain Chem Pharm 21:100428. https://doi.org/10.1016/j.scp.2021.100428

Sun T, Xu Y, Sun Y et al (2021) Crayfish shell biochar for the mitigation of Pb contaminated water and soil: characteristics, mechanisms, and applications. Environ Pollut 271:116308. https://doi.org/10.1016/j.envpol.2020.116308

Suzaimi ND, Goh PS, Malek NANN et al (2019) Performance of branched polyethyleneimine grafted porous rice husk silica in treating nitrate-rich wastewater via adsorption. J Environ Chem Eng 7:103235. https://doi.org/10.1016/j.jece.2019.103235

Tang Y, Li Y, Zhan L et al (2022) Removal of emerging contaminants (bisphenol A and antibiotics) from kitchen wastewater by alkali-modified biochar. Sci Total Environ 805:150158. https://doi.org/10.1016/j.scitotenv.2021.150158

Thommes M, Kaneko K, Neimark AV et al (2015) Physisorption of gases, with special reference to the evaluation of surface area and pore size distribution (IUPAC Technical Report). Pure Appl Chem 87:1051–1069. https://doi.org/10.1515/pac-2014-1117

Tran HN, Wang Y-F, You S-J, Chao H-P (2017a) Insights into the mechanism of cationic dye adsorption on activated charcoal: the importance of π–π interactions. Process Saf Environ Prot 107:168–180. https://doi.org/10.1016/j.psep.2017.02.010

Tran HN, You S-J, Chao H-P (2017b) Fast and efficient adsorption of methylene green 5 on activated carbon prepared from new chemical activation method. J Environ Manage 188:322–336. https://doi.org/10.1016/j.jenvman.2016.12.003

Tran HN, Tomul F, Thi Hoang Ha N et al (2020) Innovative spherical biochar for pharmaceutical removal from water: insight into

adsorption mechanism. J Hazard Mater 394:122255. https://doi.org/10.1016/j.jhazmat.2020.122255

Turk Sekulic M, Boskovic N, Slavkovic A et al (2019) Surface functionalised adsorbent for emerging pharmaceutical removal: adsorption performance and mechanisms. Process Saf Environ Prot 125:50–63. https://doi.org/10.1016/j.psep.2019.03.007

Veiga PAdaS, Schultz J, da S Matos TT et al (2020) Production of high-performance biochar using a simple and low-cost method: optimization of pyrolysis parameters and evaluation for water treatment. J Anal Appl Pyrol 148:104823. https://doi.org/10.1016/j.jaap.2020.104823

Wang J, Zhang M (2020) Adsorption characteristics and mechanism of bisphenol A by magnetic biochar. Int J Environ Res Public Health 17:1075. https://doi.org/10.3390/ijerph17031075

Wang L, Ok YS, Tsang DCW et al (2020) New trends in biochar pyrolysis and modification strategies: feedstock, pyrolysis conditions, sustainability concerns and implications for soil amendment. Soil Use Manag 36:358–386. https://doi.org/10.1111/sum.12592

Werkneh AA, Gebru SB, Redae GH, Tsige AG (2022) Removal of endocrine disrupters from the contaminated environment: public health concerns, treatment strategies and future perspectives - A review. Heliyon 8:e09206. https://doi.org/10.1016/j.heliyon.2022.e09206

Xu J, Wang L, Zhu Y (2012) Decontamination of bisphenol A from aqueous solution by graphene adsorption. Langmuir 28:8418–8425. https://doi.org/10.1021/la301476p

Yan Y, Manickam S, Lester E et al (2021) Synthesis of graphene oxide and graphene quantum dots from miscanthus via ultrasound-assisted mechano-chemical cracking method. Ultrason Sonochem 73:105519. https://doi.org/10.1016/j.ultsonch.2021.105519

Yang X, Zhang X, Ngo HH et al (2022) Sorptive removal of ibuprofen from water by natural porous biochar derived from recyclable plane tree leaf waste. J Water Process Eng 46:102627. https://doi.org/10.1016/j.jwpe.2022.102627

Zanella HG, Spessato L, Lopes GKP et al (2021) Caffeine adsorption on activated biochar derived from macrophytes (Eichornia crassipes). J Mol Liq 340:117206. https://doi.org/10.1016/j.molliq.2021.117206

Zbair M, Bottlinger M, Ainassaari K et al (2020) Hydrothermal carbonization of argan nut shell: functional mesoporous carbon with excellent performance in the adsorption of bisphenol A and diuron. Waste Biomass Valor 11:1565–1584. https://doi.org/10.1007/s12649-018-00554-0